

COVER PAGE

Document downloaded by @DAEL

Sat Nov 28 22:28:17 2026
For personal use

When automatic English translation is provided, only the original document is authentic.
The EAA cannot be held responsible of any translation error

Bibliographical reference

Theoretical and Experimental Investigation on Laser-Generated Guided Wave Propagation Characteristic of an Overlying Plate/Substrate, Hao Wang, Qingbang Han and Menglu Qian, Acta Acustica **vol. 99** (Number 5), 2013, pp. 687-693

DOI
https://doi.org/10.3813/AAA.918647

ACTA ACUSTICA UNITED WITH ACUSTICA
Vol. 99 (2013) 687 – 693

Scientific Papers
DOI 10.3813/AAA.918647

Theoretical and Experimental Investigation on Laser-Generated Guided Wave Propagation Characteristic of an Overlying Plate/Substrate

Hao Wang[1)], Qingbang Han[2)], Menglu Qian[1)]

[1)] Institute of Acoustics, Tongji University, Shanghai 200092, China.

[2)] Changzhou Key Laboratory of Sensor Networks and Environmental Sensing, Hohai University, Changzhou 213022, China. hqb0092@163.com

Summary

We report theoretical and experimental investigations of guided waves on an overlying plate/substrate (Aluminum plate / Plexiglas) surface. Three types of waves, i.e., S_0-like, A_0-like and Rayleigh-like modes are analyzed numerically under different boundary conditions of slip, weld, and the spring model. By studying the spring constants K_T dependence of the A_0-like mode dispersion, the most sensitive area is found to be located in range of 10^{11}–10^{14} Pa/m. The simulated transient displacement response by inverse Fourier transforms is in good agreement with the experimental results. Dispersion estimations of guided wave demonstrate its feasibility to inverse K_T, which is possible to be used to the bonding characteristic evaluation.

PACS no. 43.20.Hq, 43.20.Mv

1. Introduction

Thin layers bonded on the substrate materials are widely used in the fields of microelectronics, automotive and aerospace industries for protection or other purposes [1, 2, 3, 4]. In these applications, the ultrasonic technology is often used to test the material or bonding quality, which reduces the inspection range of guided wave NDE techniques. When the length scale of the roughness feature of the mating surfaces is much smaller than the wavelength of the elastic wave considered, the contact interface behaves as a spring-type interface that has equivalent stiffness in the normal direction, K_N, and in the tangential direction, K_T [5, 6] . Generally, the adhesive layer is much thinner than adherent layers, the thickness influence usually ignored [7, 8] except when the wave is propagating through a three-layer sandwich with the middle layer representing the adhesive layer [9, 10, 11]. The wave propagation characteristics in coatings have been widely stuided [12, 13], in this case ,the coatings are so thin that only one mode, i.e., the SAW (surface acoustic wave), could be experimentally detected. To characterize the thin film, the laser ultrasonics are widely applied in detection for its advantages of a wide frequency band and high resolution [14, 15, 16]. This paper is devoted to the wave propagation characteristics on a surface of thin metal (aluminum) plate bonded on a substrate (Plexiglas) specimen, where the simplified two layers model including the substrate and thin plate can be applied since the thickness of the plate is much larger than that of bonding layer. Different from the SAW wave in the coatings, many modes such as A-like, S-like and Rayleigh-like modes are excited, which have not been extensively studied by other groups. The other motivation is to investigate the possibility of evaluation of the adhesion interface property by using the guided wave. For these purposes, a nanosecond pulsed Nd:YAG laser is used to excite waves on metal surface, in situ the normal displacement signals are detected by a photorefractive interferometer and the dispersion estimations of guided wave are also performed.

Received 10 December 2012,
accepted 12 June 2013.

2. Theory mode

2.1. Problem presentation

An overlying plate /substrate model (an isotropic homogeneous semi-infinite medium covered with an overlying plate) illuminated by a laser pulse is depicted in Figure 1, where $z = 0$ presents the interface and x indicates the propagation direction of the guided waves; the overlying plate is homogenous, isotropic, and linearly elastic. The mode could be classified into the case of fast on slow; the situation is complicated by the probable presence of the cutoff velocity occurring at transverse wave velocity of the substrate [17].

2.2. Equations of motion

In the horizontal coordinate system, the displacement can be expressed by the potential functions ϕ_i and ψ_i ($i = 1, 2$), where the subscripts 1 and 2 denote the overlying plate and the substrate respectively.

© S. Hirzel Verlag · EAA

Displacement potentials satisfy the Helmholtz equations

$$\begin{cases} \nabla^2\phi = \frac{\partial^2\phi}{c_L^2\partial t^2}, \\ \nabla^2\psi_y = \frac{\partial^2\psi_y}{c_S^2\partial t^2}, \end{cases} \tag{1}$$

where c_L and c_S are the longitudinal and shear velocities in the media. Applying the Fourier transforms to space x and time t in equation (1) (are presented with $-$ and *), yields the equations

$$\begin{cases} \dfrac{\partial^2\phi}{z^2} = \left(k^2 - \dfrac{\omega^2}{c_L^2}\right)\overline{\phi}^*, \\ \dfrac{\partial^2\psi_y}{z^2} = \left(k^2 - \dfrac{\omega^2}{c_S^2}\right)\overline{\psi}_y^*. \end{cases} \tag{2}$$

The appropriate solutions in a transform domain can be obtained as

$$\begin{cases} \overline{\phi}^* = A\mathrm{e}^{-k_\alpha z} + B\mathrm{e}^{k_\alpha z}, \\ \overline{\psi}_y^* = C\mathrm{e}^{-k_\beta z} + D\mathrm{e}^{k_\beta z}, \end{cases} \tag{3}$$

with $k = \omega/c$,

$$k_\alpha = \sqrt{k^2 - \frac{\omega^2}{c_L^2}}, \quad k_\beta = \sqrt{k^2 - \frac{\omega^2}{c_S^2}}.$$

The displacement and stress are given by

$$\begin{cases} u_z = \dfrac{\partial\phi}{\partial z} + \dfrac{\partial\psi_y}{\partial x}, \\ u_x = \dfrac{\partial\phi}{\partial x} - \dfrac{\partial\psi_y}{\partial z}, \\ \sigma_{zz} = \lambda\left(-\dfrac{\omega^2}{c_L^2}\right) + 2\mu\left(\dfrac{\partial^2\phi}{\partial z^2} + \dfrac{\partial^2\psi_y}{\partial z\partial x}\right), \\ \sigma_{zx} = \lambda\left(2\dfrac{\partial^2\psi_y}{\partial z\partial x} - \dfrac{\partial^2\psi_y}{\partial z^2} + \dfrac{\partial^2\psi_y}{\partial x^2}\right). \end{cases} \tag{4}$$

Applying the Fourier transforms to equation (4), gives

$$\begin{cases} \overline{u_z}^* = -k_\alpha\mathrm{e}^{-k_\alpha z}A + k_\alpha\mathrm{e}^{k_\alpha z}B + \mathrm{i}k\mathrm{e}^{-k_\beta z}C + \mathrm{i}k\mathrm{e}^{k_\beta z}D, \\ \overline{u_x}^* = \mathrm{i}k\mathrm{e}^{-k_\alpha z}A + \mathrm{i}k_\alpha\mathrm{e}^{k_\alpha z}B + k_\beta\mathrm{e}^{-k_\beta z}C - k_\beta\mathrm{e}^{k_\beta z}D, \\ \overline{\sigma_{zz}}^* = \mu\Big[\left(2k^2 - \dfrac{\omega^2}{c_S^2}\right)\mathrm{e}^{-k_\alpha z}A + \left(2k^2 - \dfrac{\omega^2}{c_S^2}\right)\mathrm{e}^{k_\alpha z}B \\ \qquad -2\mathrm{i}kk_\beta\mathrm{e}^{-k_\beta z}C + 2\mathrm{i}kk_\beta\mathrm{e}^{k_\beta z}D\Big], \\ \overline{\sigma_{zx}}^* = \mu\Big[-2\mathrm{i}kk_\alpha\mathrm{e}^{-k_\alpha z}A + 2\mathrm{i}kk_\alpha\mathrm{e}^{k_\beta z}B \\ \qquad -\left(2k^2 - \dfrac{\omega^2}{c_S^2}\right)\mathrm{e}^{-k_\beta z}C + \left(2k^2 - \dfrac{\omega^2}{c_S^2}\right)\mathrm{e}^{k_\beta z}D\Big]. \end{cases} \tag{5}$$

The stress on the overlying plate surface can be written as

$$\overline{\sigma_{zz1}}^*\big|_{z=d} = G(k)\,F(\omega), \qquad \overline{\sigma_{zx1}}^*\big|_{z=d} = 0, \tag{6}$$

where $G(k)$ and $F(\omega)$ are transform domain expression of the excitation source. The mechanical boundary conditions at a 'general bonding' interface $z = 0$ can be given

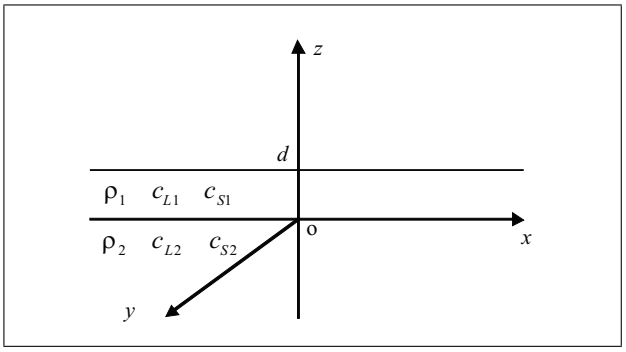

Figure 1. The coordinate axes of a metal overlying plate / substrate model.

by

$$\begin{cases} \overline{\sigma_{zz1}}^*\big|_{z=0} = \overline{\sigma_{zz2}}^*\big|_{z=0}, \\ \overline{\sigma_{zx1}}^*\big|_{z=0} = \overline{\sigma_{zx2}}^*\big|_{z=0}, \\ \overline{\sigma_{zz1}}^*\big|_{z=0} = K_N\left(\overline{u_{z1}}^*\big|_{z=0} - \overline{u_{z2}}^*\big|_{z=0}\right), \\ \overline{\sigma_{zx1}}^*\big|_{z=0} = K_T\left(\overline{u_{x1}}^*\big|_{z=0} - \overline{u_{x2}}^*\big|_{z=0}\right), \end{cases} \tag{7}$$

where K_N and K_T are normal and tangent distributed spring constants (N/m^3), respectively. Substituting equations (5),(6) into equation (7) we have

$$\left[\,M_K\,\right]\begin{bmatrix} A_1 \\ B_1 \\ C_1 \\ D_1 \\ B_2 \\ D_2 \end{bmatrix} = \begin{bmatrix} 0 \\ 0 \\ 0 \\ 0 \\ G(k)F(\omega) \\ 0 \end{bmatrix}, \tag{8}$$

where

$$M_K = \begin{bmatrix} -k_{\alpha1} & k_{\alpha1} & \mathrm{i}k \\ \mathrm{i}k & \mathrm{i}k & k_{\beta1} \\ 2k^2 - \frac{\omega^2}{c_{\beta1}^2} & 2k^2 - \frac{\omega^2}{c_{\beta1}^2} & -2\mathrm{i}kk_{\beta1} \\ -2\mathrm{i}kk_{\alpha1} & 2\mathrm{i}kk_{\alpha1} & -\left(2k^2 - \frac{\omega^2}{c_{\beta1}^2}\right) \\ \left(2k^2 - \frac{\omega^2}{c_{\beta1}^2}\right)p & \left(2k^2 - \frac{\omega^2}{c_{\beta1}^2}\right)\frac{1}{p} & -2\mathrm{i}kk_{\beta1} \\ -2\mathrm{i}kk_{\alpha1}p & 2\mathrm{i}kk_{\alpha1}\frac{1}{p} & -\left(2k^2 - \frac{\omega^2}{c_{\beta1}^2}\right)q \end{bmatrix}$$

$$\begin{matrix} \mathrm{i}k & -\left[k_{\alpha2} + \frac{\mu_2}{K_N}\left(2k^2 - \frac{\omega^2}{c_{\beta1}^2}\right)\right] \\ -k_{\beta1} & -\left[\mathrm{i}k + \frac{\mu_2}{K_T}\left(2\mathrm{i}kk_{\alpha2}\right)\right] \\ 2\mathrm{i}kk_{\beta1} & -\mu_{21}\left(2k^2 - \frac{\omega^2}{c_{\beta2}^2}\right) \\ -\left(2k^2 - \frac{\omega^2}{c_{\beta1}^2}\right) & -\mu_{21}2\mathrm{i}kk_{\alpha2} \\ 2\mathrm{i}kk_{\beta1}\frac{1}{q} & 0 \\ -\left(2k^2 - \frac{\omega^2}{c_{\beta1}^2}\right)\frac{1}{q} & 0 \end{matrix}$$

$$\begin{bmatrix} -\left[\mathrm{i}k + \frac{\mu_2}{K_T}\left(2\mathrm{i}kk_{\beta 2}\right)\right] \\ k_{\beta 2} + \frac{\mu_2}{K_N}\left(2k^2 - \frac{\omega^2}{c_{\beta 2}^2}\right) \\ -\mu_{21} 2\mathrm{i}kk_{\beta 2} \\ \cdots \quad \mu_{21}\left(2k^2 - \frac{\omega^2}{c_{\beta 2}^2}\right) \\ 0 \\ 0 \end{bmatrix}$$

and $p = \mathrm{e}^{-k_{\alpha 1}d}$, $q = \mathrm{e}^{-k_{\beta 1}d}$.

2.3. The characterization equation and transient response of waves

The characterization equation can be derived from equation (8) under the condition

$$\det\left(M_K\right) = 0. \tag{9}$$

Applying the limits that K_N and $K_T \to \infty$ or $K_T \to 0$, equation (4) will be reduced to the characteristic equation of interface waves at welded or slip boundaries, respectively.

The normal displacement of overlying plate surface in transforms domain can be written as

$$\begin{aligned} \overline{u_{z1}}^* \big|_{z=d} = & -k_{\alpha 1}\mathrm{e}^{-k_{\alpha 1}d}A_1 + k_{\alpha 1}\mathrm{e}^{-k_{\alpha 1}d}B_1 \\ & + \mathrm{i}k\mathrm{e}^{-k_{\beta 1}d}C_1 + \mathrm{i}k\mathrm{e}^{-k_{\beta 1}d}D_1 \end{aligned} \tag{10}$$

The transient displacement can be obtained by inverse Fourier transform,

$$\overline{u_{z1}}\big|_{z=d} = \int_{-\infty}^{\infty}\left(\int_{-\infty}^{\infty}\overline{u_{z1}}^*\mathrm{e}^{-\mathrm{i}kx}\mathrm{d}k\right)\mathrm{e}^{\mathrm{i}\omega t}\mathrm{d}\omega. \tag{11}$$

3. Guided mode analysis

3.1. Riemann analysis of the equation

Equation (9) contains four square roots, i.e.

$$k_{\alpha 1} = \sqrt{\frac{\omega^2}{c_{L1}^2} - k^2}, \qquad k_{\beta 1} = \sqrt{\frac{\omega^2}{c_{S1}^2} - k^2},$$
$$k_{\alpha 2} = \sqrt{\frac{\omega^2}{c_{L2}^2} - k^2}, \qquad k_{\beta 2} = \sqrt{\frac{\omega^2}{c_{S2}^2} - k^2}.$$

The latter two may lead to multivalued results due to complex roots [18]. It may be written on two Riemann sheets which correspond to the square roots with a positive real part and a negative real part. The Riemann surface for the equation (9) also has four sheets which are designated by a group of two signs $(\pm, \pm)$. Each of the signs stands for the Riemann sheet of $(k_{\alpha 2}, k_{\beta 2})$ and so the equation (9) gives rise to four separate functions. When the velocity corresponds to the Riemann sheet with sign $(+, +)$ it is slower than the shear velocity in substrate (c_{S2}) and the roots are real. There exist a cutoff at c_{S2}, if the velocity faster than c_{S2}, the Riemann sheets will change in sign $(-, +)$ or $(-, -)$ and the roots become complex number and leaky wave appears. Some roots may be missed if Riemann analyses are not taken into consideration.

When the guided wave is propagating along x direction, leaky waves may exist, and the corresponding roots are complex, i.e., $c = c_R - c_I\mathrm{i}$, where C_R, c_I denote the real part and imaginary part of the complex velocity respectively. The phase velocity c_p and attenuation α are defined as $c_p = \omega/\Re e\{k\} = c_R + v_I^2/c_R$ and $\alpha = \Im m\{k\} = c_I\omega/(c_R^2 + c_I^2)$.

Table I. The material parameters used for theoretical analysis. ρ: density (kg/cm^3), L: Longitudinal wave (m/s), S: Shear wave (m/s), d: thickness (mm).

materials	ρ	L	S	d
Aluminum	2700	6260	3080	0.95
Plexiglass	1140	2660	1250	-

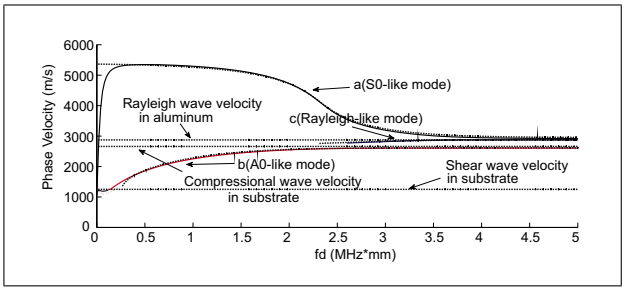

Figure 2. Dispersion of guided wave, the solid and dotted line represent the weld and slip boundary condition respectively.

3.2. Numerical results and analysis on dispersion and attenuation

Table I illustrates the parameters used for theoretical analysis when the medium of the overlying plate and substrate are Aluminum and Plexiglas, respectively.

The dispersion curves of guided wave calculated form equation (9) are plotted in Figure 2, in which (a), (b) and (c) denote the three kinds of guided wave modes, and the solid and dotted line express the weld and slip boundary conditions, respectively. The excited modes are dispersive, and the differences are obvious in low-frequency range ($f^*d < 0.3\,\mathrm{MHz\,mm}$). However, in the high-frequency range, since the wave energy is mainly concentrated in the metal plate, the dispersion effect becomes weaker and weaker. The curve (b) and (a), which are referred as S_0-like and A_0-like mode in this paper, are similar to a Lamb wave mode in a single plate. The curve (c) implies the Rayleigh-like wave. The S_0 – like mode and Rayleigh-like waves are located in Riemann sheet $(-, -)$ due to their velocities exceeding that of the substrate longitudinal wave. As the value of frequency * thickness (fd) increasing, the S_0-like mode and Rayleigh-like wave approach the Rayleigh velocity of Al, while the A_0-like mode

approaches longitudinal velocity of the substrate, which are different from the A_0 of Lamb wave (it converges to Rayleigh velocity). When the velocity of the A_0-like mode exceeds the shear velocity of the substrate, the Riemann sheet transforms from sign $(+,+)$ to $(-,+)$. Moreover, there exists a cutoff frequency for the Rayleigh-like mode, which implies the wave cannot be excited if the excitation frequency is not high enough.

The attenuation characteristics of three modes are described in Figure 3. It is shown that the attenuation of the A_0-like and S_0-like increases as a function of fd, and A_0-like mode attenuation is very small under slip boundary condition. The Rayleigh-like mode attenuation is also small and displays a sloping downward trend.

As the matter of fact, the normal displacement can be treated as continuous and the difference is more obvious in tangential direction. The dispersion curves of A_0-like mode under the condition of $K_N \to \infty$ and $K_T \in (0, \infty)$ in the low-frequency range ($fd < 0.3$ MHz mm, lower than cutoff) are plotted in Figure 4. In this case, the complex roots do not exist, and only one mode can propagate.

It can be found that dispersion characteristics are related to K_T, and the most sensitive range of K_T is between 10^{11} and 10^{14} Pa/m/s. The frequency is also different when its velocity approaches shear velocity of substrate.

Besides interface boundary condition, the guided wave dispersion also depends on parameters of overlying plate and substrate, such as density or bulk velocity. Figure 5 shows relative dispersion change rate caused by 5% variation in density, longitudinal and shear velocity of overlying plate and substrate.

It was found in the lower frequency range, which the dispersion curves rely crucially on the shear velocity of substrate, which should be delicately treated when the K_T is inversed.

3.3. Simulation of guided wave transient response

For comparison purpose, we simulate guided wave transient response through inversion of equation (10). The source as a function time and space in the transform domain is chosen as

$$g(x) = \frac{1}{\sqrt{\pi}a} e^{-(x/a)^2} \quad \text{and} \quad f(t) = \frac{t}{t_0} e^{-t/t_0},$$

with $a = 0.2$ mm and $t_0 = 4$ ns.

For an Aluminum / Plexiglas specimen, the transient displacement response at 20 mm distance from the excitation source is plotted in Figure 6, where the solid line and dotted line indicate weld and slip interface bonding, respectively.

The S_0-like, Rayleigh-like and A_0-like modes can be identified via their arrival times, where the S_0-like mode has the fastest propagation velocity and the smallest amplitude, and A_0-like mode has the longest arrival time. The wave form of S_0-like, Rayleigh-like is almost overlapping for two boundary conditions, while A_0-like mode shows an obvious difference. For A_0-like mode, it seems the wave form in weld condition advances the slip condition. Both

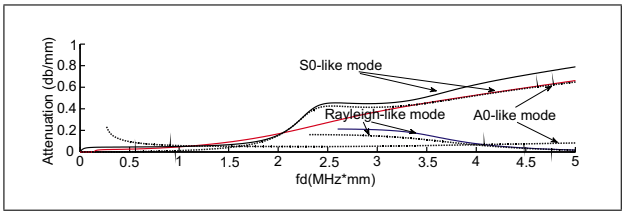

Figure 3. Attenuation of guided wave versus Frequency * Thickness.

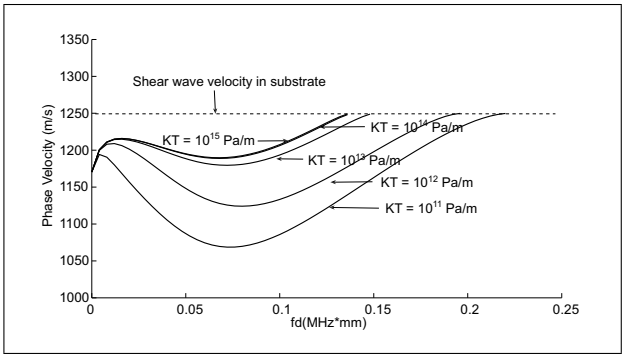

Figure 4. Dispersion dependence on K_T with $K_N \to \infty$.

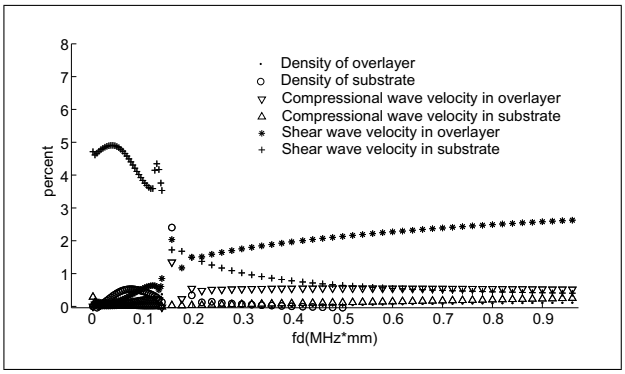

Figure 5. Relative dispersion change rate caused by 5% variation in density, longitudinal and shear velocity of overlying plate and substrate.

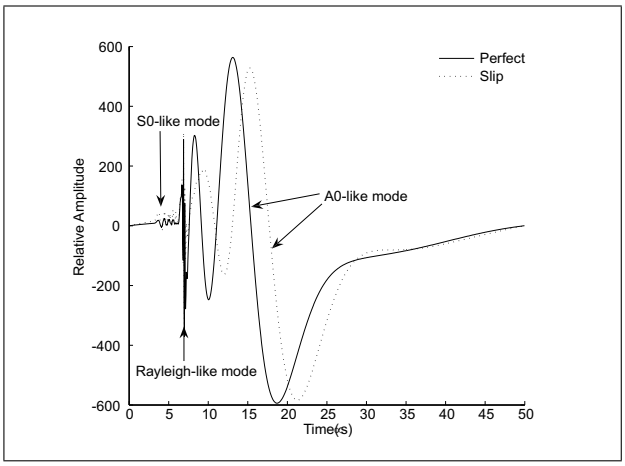

Figure 6. Transient displacement response at 20 mm distance away the excitation source.

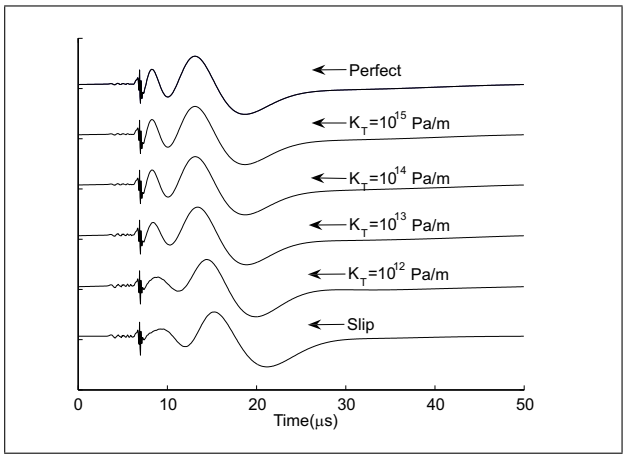

Figure 7. Transient response based on spring connect mode, the receive position is 20 mm away from the source.

signals are dispersive and high frequency component propagates faster than low frequency component, which is in accordance with the results in Figure 2.

Figure 7 describes the transient response in the case of $K_N \to \infty$ and different K_T value, the A_0-like mode varies as the function of tangent distributed spring constant. The Rayleigh-like and S_0-like mode are weakly influenced by spring constant K_T, and the larger value of K_T, the more antedisplacement of A_0 wave peak.

4. Experimental results and discussion

4.1. Experimental setup

The schematic diagram of the experimental setup is shown in Figure 8. A 0.95 mm thick, 4 cm wide and 10 cm long Aluminum is deposited on a plexiglas sample. A pulse laser (532 nm, 4.2 ns) is focused on the surface of the metal with a cylindrical lens and a line source of 18 mm long and 0.2 mm wide is formed. The ablation effect is induced on the surface of the Aluminum for higher laser energy, which could be equivalent to the normal force source. The probe laser beam of a photorefractive interferometer (TEMPO-FS200, 532 nm) is applied to detect the displacement on the surface of Al. The output signal of interferometer is recorded by an oscilloscope and averaged over 64 laser shots to improve the signal to noise ratio. For each propagation direction of interface waves, more than 12 signals are continually collected as the distance between laser source and probe beam changes in step of 1 mm.

In the experiment, the slip interface is formed with pure water coupling; the weld connection is formed with epoxy bonding for a long time and different tangent distributed spring constants are simulated approximately with epoxy solidifying in different time. The experimental material parameters are listed in Table I, the plate thickness is measured with Vernier caliper, and the relative error is less than 1%; the velocity of materials is measured using pulse echo method, and the relative error is no more than 2%.

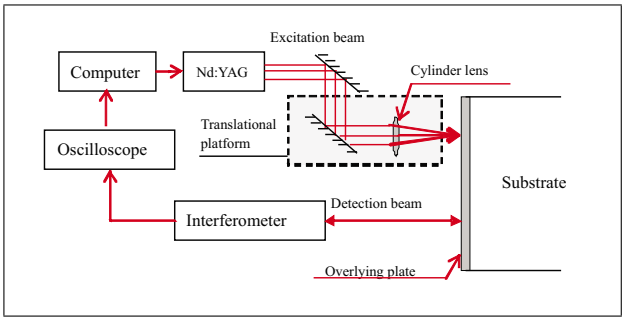

Figure 8. Schematic diagram of the experimental setup.

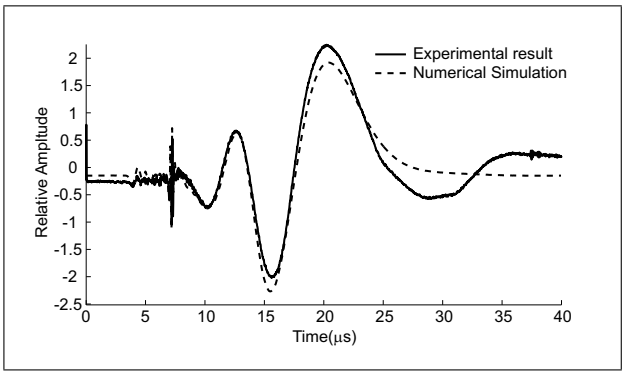

Figure 9. Waveform on Alumium/Plexiglass construction for lip interface. Solid line: experimental result, dotted line: numerical simulation.

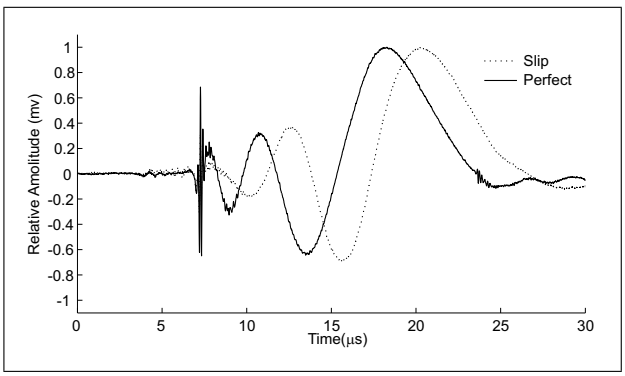

Figure 10. Experimentally detected signals for slip and perfect interface connection.

4.2. Measurement results

In Figure 9 the solid line represents a typical signal collected by a digital oscilloscope in experiment at 21 mm distance from source in the case of slip interface, which is in good agreement with the numerical simulation plotted in dotted line.

Figure 10 shows the experimental signals for slip and perfect interface connection; the experimental results are consistent with the theoretical predications shown in Figure 6.

When an Aluminum plate is adhered to Plexiglas using Epoxy, K_T can be used to specify the interface connection variation in the process of Epoxy solidifying, and K_T increases with the solidifying time. Figure 11 shows the

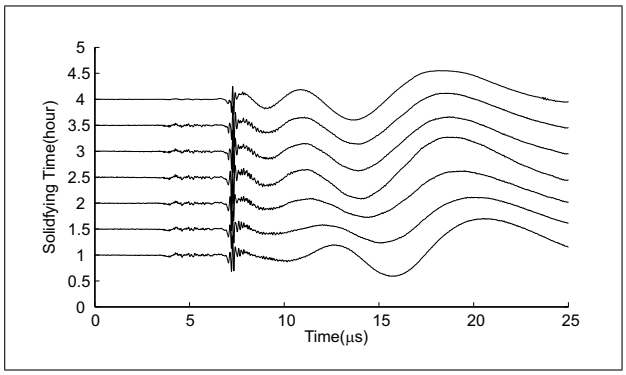

Figure 11. Detected waveform against solidifying time, the detection position is 21 mm from source.

signals corresponding to different solidifying time every half an hour.

It is shown that there is not obvious change for S_0-like and Rayleigh-like mode, and waveform of A_0-like shifts forward as a function of the solidifying time; the wave characteristics are similar to those shown in Figure 7, which demonstrates the feasibility of simulation K_T with solidifying time method.

4.3. Guided wave dispersion estimation

Many methods have been developed for wave dispersion estimation [19, 20], which is necessary for parameter inversion. In this paper, the expanded Prony's method is used.

Three kinds of detection signals with different velocities are head-to-tail in sequence, where the fastest is S_0-like mode; the slowest is A_0 -like mode. Experimental signals showed amplitude of the S_0-like mode is much smaller, to avoid possible saturation of the A_0-like and Rayleigh-like signals? the S_0-like mode was processed as noise in dispersion estimation. Thus, only one mode exists at one frequency. Using the array detection signals, we performed dispersion estimation to guided wave for Figure 12.

Two mode waves can be identified clearly, in the lower-frequency range the phase velocity of first mode increases with fd exponentially, compared with Figure 2 ,it can be identified as A_0–like mode. The second mode can be identified as Rayleigh-like because its velocity 2.915 μs/m, is closed to the theoretical value 2.921 μs/m, and shows little dispersion.

Figure 13 shows guided wave dispersion in process of epoxy solidifying, the red and black dots represent the dispersion of slip ($K_T = 0$) and weld connection ($K_T = \infty$), the blue and green dots indicate the solidifying condition at solidifying beginning and two hour later, respectively. The general characters of guided wave are in agreement with theory. The dispersion of guided wave detected immediately after solidifying is closed to the slip condition, the dispersion detected two hour later almost overlaps with the weld connection and the K_T variation can be simulated as a function of solidifying time. Inversing K_T by using dispersion estimation is in progress.

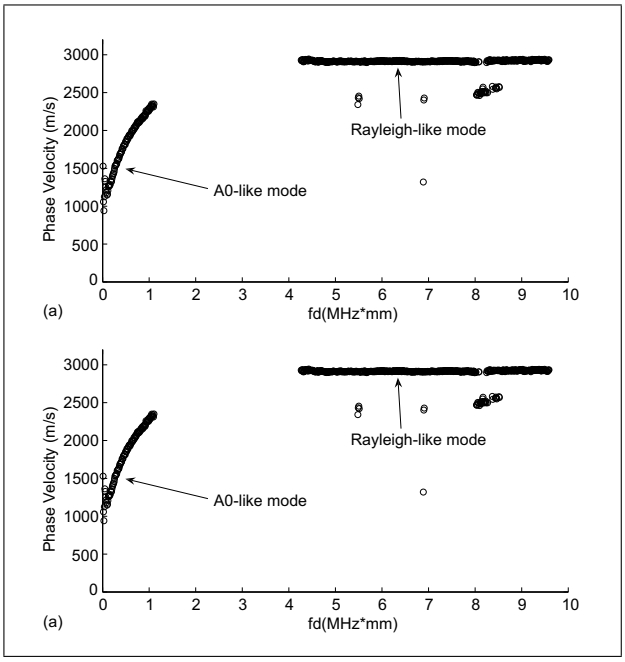

Figure 12. Experimentally obtained dispersion curves by expanded Prony's method (a) slip interface (b) weld interface.

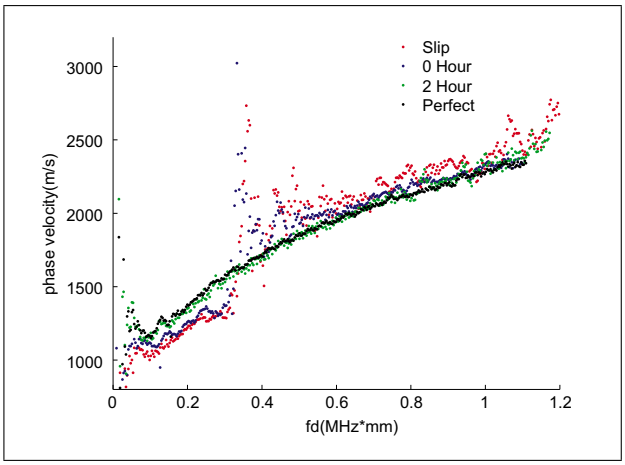

Figure 13. Guided wave dispersion in process of epoxy solidifying.

5. Conclusion

In this study, the laser-ultrasonic generation of guided waves on metal overlying plate / substrate (Aluminum plate / Plexiglas) surface is investigated both theoretically and experimentally. A Fourier transform is applied in the time and space domains, and the characterization equation is established via the introduction of spring boundary. Through Riemann analysis, the existence of three types of wave ie. S_0-like, A_0-like and Rayleigh-like modes are predicted numerically; and the dispersion of A_0-like mode depended on K_T is calculated, whose most sensitive range is located in range of 10^{11}–10^{14} Pa/m. The transient displacement response is simulated by means of inverse Fourier transforms, it is shown that the Rayleigh-like and S_0-like modes are weakly influenced by the spring constant K_T,

while A_0 waveform depends strongly on K_T. The guided waves are measured by means of laser ultrasonics, the experimental results fit theoretical predictions well. Dispersion estimations of guided waves show that the A_0–like and Rayleigh-like are detected successfully and can be applied in parameter K_T inversion.

Acknowledgement

This work was supported by the Fundamental Research Funds for the Central Universities of Hohai University (No: 2011B11014), the Natural Science foundation of China Grant Nos. 11104205, 10834009 and 11274091.

References

[1] L. De Lorenzis, J. G. Teng, L. Zhang: Interfacial stresses in curved members bonded with a thin plate. International Journal of Solids and Structures **43** (2006) 7501–7517.

[2] E. M. Palmeira, J. Tatto, G. L. S. Araujo: Sagging and filtration behaviour of nonwoven geotextiles overlying different bedding materials. Geotextiles and Geomembranes **31** (2012) 1–14.

[3] B. B. Adhikary, H. Mutsuyoshi, M. Sano: Shear strengthening of reinforced concrete beams using steel plates bonded on beam web: experiments and analysis. Construction and Building Materials **14** (2000) 237–244.

[4] J.-Y. Sener, F. Delannay: On the transition between adhesive and cohesive modes of debonding during peeling of thin plates bonded with an epoxide adhesive. International Journal of Adhesion and Adhesives **21** (2001) 339–348.

[5] B. W. Drinkwater, R. S. Dwyer-Joyce, P. Cawley: A study of the intraction between ultrasound and a partially contacting solid Űsolid interface. Proc. Roy. Soc. Lond. A **452** (1996) 2613–2628.

[6] P. B. Nagy: Ultrasonic classification of imperfect interfaces. J. Nondestruct. Eval. **11** (1992) 127–139.

[7] R. O. Claus: Adhesive bondline interrogation use stoneley wave methods. J. Appl. Phys. **50** (1979) 8066–8069.

[8] A. I. Lavrentyev, J. T. Beals: Ultrasonic measurement of the diffusion bond strength. Ultrasonics **38** (2000) 513–516.

[9] N. A. Ismaili, D. Chenouni, Z. Lakhliai, M. Ech-Bherif El-Kettani, B. Morvan, J.-L. Izbicki: Determination of epoxy film parameters in a three-layer metal/ adhesive/ metal structure. IEEE Transactions on ultrasonics,ferroeiectrics, and frequency control **56** (2009) 1955–1959.

[10] S. I. Rokhlin, Y. J. Wang: Analysis of boundary conditions for elastic wave interaction with an interface between two solids. J. Acoust. Soc. Am. **89** (1991) 503–515.

[11] L. Singher: Bond strength measurement by ultrasonic guided waves. Ultrasonics **35** (1997) 3055–315.

[12] Y. Zhao, X. M. Li, L. Lin, M. K. Lei: Measurements of coating density using ultrasonic reflection coefficient phase spectrum. Ultrasonics **51** (2011) 596–601.

[13] G. Wenmin, C. Glorieux, W. Lauriks, J. Thoen: Investigation of titanium nitride coating by broadband laser ultrasonic spectroscopy. Chinese Physics **11** (2002) 132–137.

[14] G. Rose, P. Psyllaki, R. Oltra, S. Costil, C. Coddet: Simultaneous laser generation and laser ultrasonic detection of the mechanical breakdown of a coating/substrate interface. Ultrasonics **39** (2001) 355–365.

[15] T. W. Murray, Z. Gao, S. Krishnaswarmy, J. D. Achenbach: Laser ultrasonic investigation of film and hard coatings. Review of Progress in Quantitative Nondestructive Evaluation (2000) 1309–1316.

[16] Q. Han, M. Qian, H. Wang: Investigation of liquid/solid interface waves with laser excitation and photoelastic effect detection. Journal of Applied Physics **100** (2006) 093101.

[17] P. Zinin, O. Lefeuvre, G. A. D. Briggs: Anomalous behavior of leaky surface waves for stiffening layer near cutoff. J. Applied Physics **82** (1997) 1031–1035.

[18] F. Padilla, M. de Billy, G. Quentin: Theoretical and experimental studies of surface waves on solid-fluid interfaces when the value of the fluid sound velocity is located between the shear and the longitudinal ones in the solid. J. Acoust. Soc. Am. **106** (1999) 666–673.

[19] D. Alleyne, P. Cawley: A two-dimensional Fourier transform method for the measurement of propagating multimode signals. J. Acoust. Soc. Am. **89** (1991) 1159–1168.

[20] W. Go, C. Glorieux, J. Thoen: Laser ultrasonic study lamb waves: determination of the thickness and velocities of a thin plate. International Journal of Engineering Science **41** (2003) 219–228.